Size Control of Monodispersed Pt Nanoparticles and Their 2D Organization by Electrophoretic Deposition

T. Teranishi, M. Hosoe, T. Tanaka, and M. Miyake*

School of Materials Science, Japan Advanced Institute of Science and Technology, 1-1 Asahidai, Tatsunokuchi, Nomi-gun, Ishikawa 923-1292, Japan

Received: August 25, 1998; In Final Form: March 9, 1999

We describe a simple method to control the size of Pt nanoparticles with the use of an alcohol reduction. They then are assembled on the electrode by an electrophoretic deposition. The mean diameter of monodispersed Pt nanoparticles can be controlled from 19 to 33 Å in one-step reaction by changing the kind and/or the concentration of alcohol in water and the amount of protective polymer, poly(*N*-vinyl-2-pyrrolidone) (PVP). The monodispersed Pt nanoparticles of smaller diameter are obtained in the order of methanol > ethanol > 1-propanol, indicating that a faster reduction rate of $[PtCl_6]^{2-}$ ions is an important factor to produce the smaller particles. The particle diameter decreases linearly with concentration of alcohol in water. Furthermore, increasing the amount of PVP makes the size of Pt nanoparticles smaller, the size distribution remaining quite narrow. By the combination of the one-step reaction with the stepwise growth reaction, Pt nanoparticles of arbitrary diameter in the range 19−50 Å can be obtained. The Pt nanoparticles obtained here have fcc structures such as bulk Pt. By using an electrophoretic deposition, more Pt nanoparticles move toward the anode with the increase of both the applied voltage and the electrophoretic time to form the Pt nanoparticle monolayer. Using the high concentration of Pt dispersion is effective to form the Pt nanoparticle monolayer.

Introduction

Nanoscale metal particles, so-called nanoparticles, hold promise for use as advanced materials with new electronic, magnetic, optic, and thermal properties[1−4] as well as new catalytic properties.[5−8] These potentialities are mainly due to the quantum size effect, which is derived from the dramatic reduction of the number of free electrons in particles in the range 1−10 nm.[9] Needless to say, an accurate control of the particle size is most important to investigate those novel physical and chemical properties. Various methods to control the size and the distribution of the nanoparticles involve micelle,[4,10,11] Langmuir−Blodgett (LB),[12] zeolite,[13] two-phase liquid−liquid,[14] and organometallic techniques.[15]

On the other hand, ordered metal nanoparticles with well-defined two- (2D) and three-dimensional (3D) spatial configurations are expected to show the novel properties that are not present in the isolated particles. The fabrication of ordered metal nanoparticles would enable us to produce surface-enhanced Raman scattering (SERS) films,[16−18] optical grating,[19,20] antireflective surface coating,[21] selective solar absorbers,[22] and data storage and microelectronics devices.[23] Two approaches have been employed in order to form 2D and 3D structures. One is to self-assemble nanoparticles by depositing a few drops of their dispersion on a substrate or by dipping it into the dispersion.[10,16,17,24−28] Recently, the formation of 2D Au and Ag monolayers using such self-assembly techniques have been reported. Another approach is to use external forces to obtain the nanoparticle monolayers, such as an electrophoretic deposition,[29] LB technique,[30] and DNA hybridization.[31] Especially, Giersig and Mulvaney demonstrated that the electrophoretic deposition is a useful technique for achieving the 2D organization of Au nanoparticles of various sizes onto a carbon-coated TEM grid.[29] The 2D and 3D arrangements of semiconductor nanoparticles such as CdSe,[32−34] CdS,[18,34−36] TiO_2,[37] and Ag_2S[11] have been also investigated by means of these techniques. Controlling the size and buildup of individual nanoparticles is also crucial in such applications as thin films. However, the Pt nanoparticle monolayer has been rarely reported,[26,38,39] probably because it is difficult to synthesize the monodispersed Pt nanoparticles.

The linear polymer and micelle are the potential candidates as protective agents to control not only the size but also the shape of the metal nanoparticles.[40,41] The formation and catalytic functionality of polymer-protected metal nanoparticles by an aqueous alcohol reduction of metal salts were first reported by Hirai and Toshima.[42] They investigated not only the catalytic activity but also the formation mechanism of the metal nanoparticles protected by poly(vinyl alcohol) or poly(*N*-vinyl-2-pyrrolidone) (PVP). The production and the catalytic activity of PVP-protected metal nanoparticles have been also studied by Bradley et al.[5] They established the method to produce the PVP-protected Pd nanoparticles by dry alcohol reduction of Pd acetate.[43] In 1995, the formation mechanism of PVP-protected Pt nanoparticles prepared in a methanol−water mixture (1/1, v/v) by methanol reduction of H_2PtCl_6, which is a system similar to ours, was investigated by Duff et al.[44] by transmission electron microscopy and UV−vis spectrophotometry, where the size of Pt nanoparticles was controlled from 15 to 40 Å with a slightly wide size distribution. Recently, we have succeeded in the synthesis of monodispersed Pd nanoparticles of 17−30 Å in mean diameter by changing the synthetic conditions systematically, i.e., the amount of PVP and the kind and/or the concentration of alcohol in the solvent as reductant.[45] Their electronic structures were revealed through ESR study.[46] Moreover, introducing the functional groups, which have high affinity for Au, to the protective polymer led to the production of fine Au nanoparticles of uniform size.[47]

In this paper, we established the method to control the size of polymer-protected Pt nanoparticles by changing the synthetic conditions systematically, which allowed us to conclude that the formation rate of Pt nuclei was an important factor to form the fine particles with a quite narrow distribution. The mono-

10.1021/jp983478m CCC: $18.00 © 1999 American Chemical Society
Published on Web 04/24/1999

dispersed Pt nanoparticles were ordered densely in 2D to obtain the Pt nanoparticle monolayers by means of an electrophoretic deposition.

Experimental Section

Materials. Hexachloroplatinic acid hexahydrate ($H_2PtCl_6 \cdot 6H_2O$, Kanto Chemicals) was used as purchased. Poly(*N*-vinyl-2-pyrrolidone) (PVP, average molecular weights (M_w) of 40 000 (Kanto Chemicals), 10 000, 29 000, 55 000, and 1 300 000 (Aldrich)) were used as a standard protective polymer for the Pt nanoparticles. Methanol, ethanol, 1-propanol, and diethyl ether were guaranteed grade and used without further purification.

Synthetic Procedure of PVP-Protected Pt Nanoparticles. A mixture of 5 mL of 6.0 mM H_2PtCl_6 aqueous solution (30 μmol of Pt), x mL of water, and y mL of alcohol ($x + y = 45$ mL) containing the designated amount of PVP was refluxed in a 100 mL flask for 3 h under air to synthesize the PVP-protected Pt nanoparticles (abbreviated as PVP-Pt). The amount of PVP was also altered from 3.33 to 133 mg (30−1200 μmol as a monomeric unit) in order to control the size and size distribution of Pt nanoparticles. The concentration of alcohol in the solvent was changed from 30 to 90 vol % in order to investigate the dependence of the size and size distribution of Pt nanoparticles on the reduction rate of $[PtCl_6]^{2-}$.

Measurements. The colloidal dispersions of the PVP-Pt nanoparticles are dark brown and stable for months at room temperature. The disappearance of $[PtCl_6]^{2-}$ ions and the formation of Pt nanoparticles were confirmed by UV−vis spectra with a Shimadzu UV-2200 UV−vis recording spectrophotometer. Fourier transform Infrared (FT-IR) spectroscopy was used to investigate an interaction between PVP and Pt during the formation process of the Pt nanoparticles by a KBr method with JASCO VALOR-III in the frequency range from 1000 to 2000 cm^{-1}. The PVP-Pt nanoparticles were characterized by transmission electron microscopy (TEM) and selected area electron diffraction (ED) at 125 kV on a Hitachi H-7100 electron microscope. Samples for TEM and ED were prepared by placing a drop of the colloidal dispersion of PVP-Pt nanoparticles onto a carbon-coated copper grid, followed by naturally evaporating the solvent. The mean diameter and standard deviation were calculated by counting 200 particles with a loupe from the TEM image of 400 000 magnifications. The crystallinity of the PVP-Pt nanoparticles was confirmed by high-resolution TEM (HRTEM) at 300 kV on a Hitachi H-9000NAR. The crystal structure of the PVP-Pt nanoparticles was also investigated by X-ray powder diffraction (XRD) on a Rigaku Rint 2000 X-ray diffractometer with Cu Kα radiation. X-ray photoelectron spectroscopy (XPS) was used to examine an electronic interaction between the N and/or O atoms of PVP and Pt during the formation of PVP-Pt nanoparticles. XPS was also employed to investigate the dependence of the atomic relaxation on the Pt particle size. The C1s, O1s, and Pt4f peaks of PVP-Pt nanoparticles with various sizes were measured on a Ulvac Phi 5600ci with monochromated Al X-ray at 350 W. Samples for FT-IR, XRD, and XPS measurements were prepared by precipitating the PVP-Pt nanoparticles with a large amount of diethyl ether, followed by filtering and drying under vacuum at 90 °C, and then crushing them with a mortar.

Electrophoretic Deposition of PVP-Pt Nanoparticles on Copper Electrode. Methanol solutions containing 0.6 mM PVP-Pt of 27.4 Å ($\sigma = 4.11$ Å) and 33.1 Å ($\sigma = 3.28$ Å) were used for the electrophoretic deposition. Both Pt nanoparticles were prepared by refluxing 30 μmol of H_2PtCl_6 in 50 cm^3 of methanol/water (9/1, v/v) mixed solution in the presence of 33.3 mg and 3.33 mg (300 μmol and 30 μmol as a monomeric unit, respectively) of PVP for 3 h, respectively. After evaporating the solvent, PVP-Pt particles were redispersed in 50 cm^3 of methanol/water mixed solution (5/5, 7/3, 10/0 (w/w)). The electrophoretic deposition of the PVP-Pt nanoparticles was carried out using 5 cm^3 of Pt colloidal dispersion in a test tube. A TEM grid coated with amorphous carbon film was pinned on a copper anode (1 cm^2). A conventional dc power supply was used to generate the applied voltage. The two copper plate electrodes were immersed into the dispersion at 2 mm spacing. After the designed electrophoretic time, the grid was removed with the voltage applied. The polarization was then turned off, and the grid was naturally dried, followed by being examined by TEM.

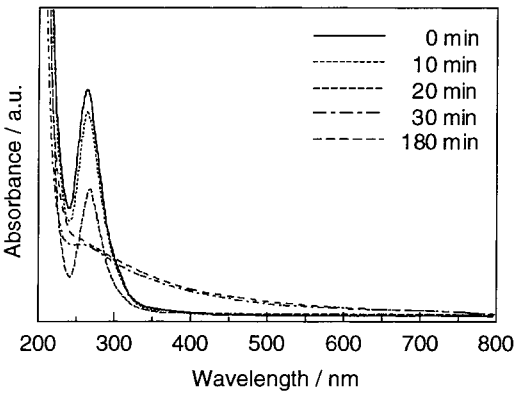

Figure 1. UV−vis spectral change during the formation of PVP-Pt nanoparticles. (PVP/Pt = 10, [methanol] = 90 vol %).

Results and Discussion

Formation of Pt Nanoparticles. The formation process of PVP-protected Pt nanoparticles (PVP/Pt = 10, mol/mol) synthesized in methanol/water (9/1, v/v) is presented as a representative example. The solution before reflux is pale yellow and shows a peak at 263.5 nm in its UV−vis spectrum due to the ligand-to-metal charge-transfer transition of the $[PtCl_6]^{2-}$ ions, as shown in Figure 1. As the refluxing time increases, the peak at 263.5 nm decreases and disappears within 30 min, indicating that the $[PtCl_6]^{2-}$ ions are completely reduced in 30 min according to the eq 1

$$H_2PtCl_6 + 2RCH_2OH \rightarrow Pt^0 + 2RCHO + 6HCl \quad (1)$$

The color of the solution turns from pale yellow into dark brown, and the absorption from the ultraviolet to the visible region increases, suggesting that the band structure of the Pt nanoparticles is formed. This broad tailing peak appeared after 30 min, and it increased with increasing refluxing time. Such tendency in UV−vis spectra is the same reported by Duff et al.[44] and suggests the formation of the Pt nanoparticles. Figure 2 presents the change in particle size of the PVP-Pt nanoparticles with increasing refluxing time. No particles were observed at 10 min, although the Pt nuclei began to form after 20 min. The size of the Pt nanoparticles formed in 30 min is almost the same as that formed in 180 min, in good agreement with the UV−vis results.

We employed UV−vis, FT-IR, and XPS measurements to clarify the protecting mechanism of PVP. As mentioned above, the mixed solution of PVP and H_2PtCl_6 before reflux shows a peak at 263.5 nm in its UV−vis spectrum due to the ligand-to-metal charge-transfer transition of the $[PtCl_6]^{2-}$ ions. On the other hand, H_2PtCl_6 solution without PVP shows a peak at 258.4 nm (Figure 3). This difference means that the ligand field

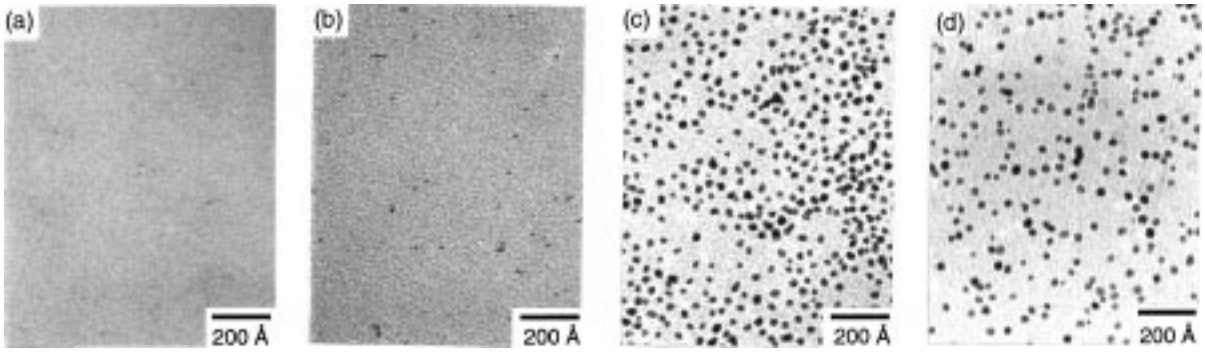

Figure 2. Change in size of PVP-Pt nanoparticles with increasing the refluxing time. The refluxing times are (a) 10 min, (b) 20 min, (c) 30 min, and (d) 180 min. (PVP/Pt = 10, [methanol] = 90 vol %).

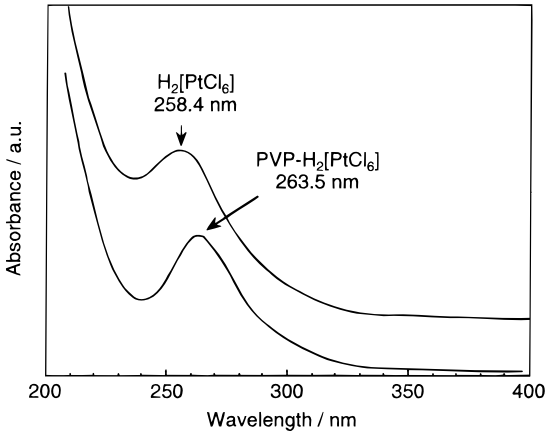

Figure 3. UV−vis spectra of $H_2[PtCl_6]$ and PVP-$H_2[PtCl_6]$. (PVP/H_2-$[PtCl_6]$ = 10).

TABLE 1: Binding Energies of N1s and O1s Orbitals of PVP, PVP-$H_2[PtCl_6]$, and PVP-Pt Nanoparticles

	binding energy, eV	
sample	N1s	O1s
PVP	399.8	531.1
PVP-$H_2[PtCl_6]$[a]	401.1	533.0
PVP-Pt	400.1	531.6

[a] Mixture of PVP and H_2PtCl_6 before reflux.

splitting of Pt5d orbital slightly expands due to the coordination of N and/or O atoms of PVP to Pt^{4+}, which provide stronger ligand field than Cl^-. In FT-IR spectra, a new peak assigned to a frequency of a carbonyl stretching band appeared at a lower frequency (1653.7 cm^{-1}) for the mixture of PVP and $H_2[PtCl_6]$ before reflux (PVP−$H_2[PtCl_6]$) in addition to that of pure PVP (1669.1 cm^{-1}), suggesting some interaction between the carbonyl groups and Pt^{4+} ions. The band for the PVP-Pt nanoparticles (1663.7 cm^{-1}) was higher than that of PVP−$H_2[PtCl_6]$, suggesting that fewer carbonyl groups interacted with the surface Pt atoms of the Pt nanoparticles. This result is comparable with the data by Hirai and Toshima,[42c] who revealed the coordination of carbonyl groups to the surface Pd atoms of PVP-protected Pd nanoparticles. Furthermore, the XPS spectra of PVP, PVP-$H_2[PtCl_6]$, and PVP-Pt nanoparticles were measured in order to investigate an electronic interaction between PVP and Pt during the formation of PVP-Pt nanoparticles. N1s and O1s binding energies of these samples are shown in Table 1. Compared to the N1s and O1s binding energies of PVP, those of PVP-$H_2[PtCl_6]$ were shifted toward higher binding energies (+1.3 and +1.9 eV, respectively), indicating that the N and O atoms of PVP were in an electron-poor state due to the coordination of these atoms to Pt^{4+} ions (a withdrawal of noncovalent electron pairs of N and O atoms by Pt^{4+} ions). Shifts in N1s and O1s binding energies were also observed for PVP-Pt (+0.3 and +0.5 eV, respectively), but the extents were rather small compared with those of PVP-$H_2[PtCl_6]$, probably because of a decrease in both an electron-withdrawing force of reduced Pt compared with Pt^{4+} and the number of Pt atoms coordinated to N and O atoms. No chlorine was detected from the PVP-Pt nanoparticles. Therefore, it is strongly suggested that the N and O atoms of PVP make coordinate bonds with Pt^{4+} ions and with parts of the surface Pt atoms of PVP-Pt.

Consequently, the formation process of the PVP-Pt nanoparticles may be summarized as follows: The PVP and $[PtCl_6]^{2-}$ ions form complexes at first through N and O atoms of PVP, which is accompanied with the elimination of some Cl^- ions from $[PtCl_6]^{2-}$. The Pt^{4+} ions are reduced to Pt^0 atoms, and the Pt nuclei form between 10 and 20 min. In the next 10 min, the reduction of Pt^{4+} and the growth of the Pt nuclei proceed at the same time to form the Pt nanoparticles with the complete elimination of Cl^-. Although the formation mechanism and the shape of the Pt nuclei are uncertain at present, the Pt nuclei may grow by reducing the Pt^{4+} ions mainly on the most catalytically active {111} surfaces of Pt nuclei to form truncated octahedral nanoparticles, as pointed out by Petroski et al.[48] Finally, the Pt nanoparticles are stabilized by the coordination of parts of the surface Pt atoms to the N and O atoms of PVP. Part of the main chain of PVP is expected to be adsorbed on the surface Pt atoms by hydrophobic interaction.

Size Control of Pt Nanoparticles by Kind and Concentration of Alcohol. We have already proven that the size of the PVP-Pd nanoparticles is greatly influenced by the kind and concentration of alcohol used as a reducing agent.[45] An appropriate choice of the kind and the concentration of the reducing agent is important in controlling the particle size, because the reduction rate of $[PtCl_6]^{2-}$ to Pt^0 are greatly affected by the kind and the concentration of the reducing agent. Figure 4 shows the mean diameters and standard deviations of the PVP-Pt nanoparticles, which were systematically synthesized by changing the kind and concentration of alcohol at the PVP/Pt ratios of 10 and 40 under reflux for 3 h. Methanol, ethanol, and 1-propanol were employed at concentrations of 30−90 vol % in solvent. From the viewpoint of the kind of alcohol, both the particle size and the standard deviation become smaller in the order of methanol > ethanol > 1-propanol at any alcohol/water ratios; this tendency corresponds to their increasing boiling points. Furthermore, from the viewpoint of the hydrogenation enthalpies of the corresponding aldehydes, methanol is unfavorable to be oxidized in comparison with ethanol and 1-propanol. Influence of the kind of alcohol on the reduction rate of $[PtCl_6]^{2-}$ is presented in Figure 5. While $[PtCl_6]^{2-}$ ions are gradually reduced by methanol, the drastic reduction of $[PtCl_6]^{2-}$ occurs in a short period in the case of 1-propanol. Thus, it is indicated

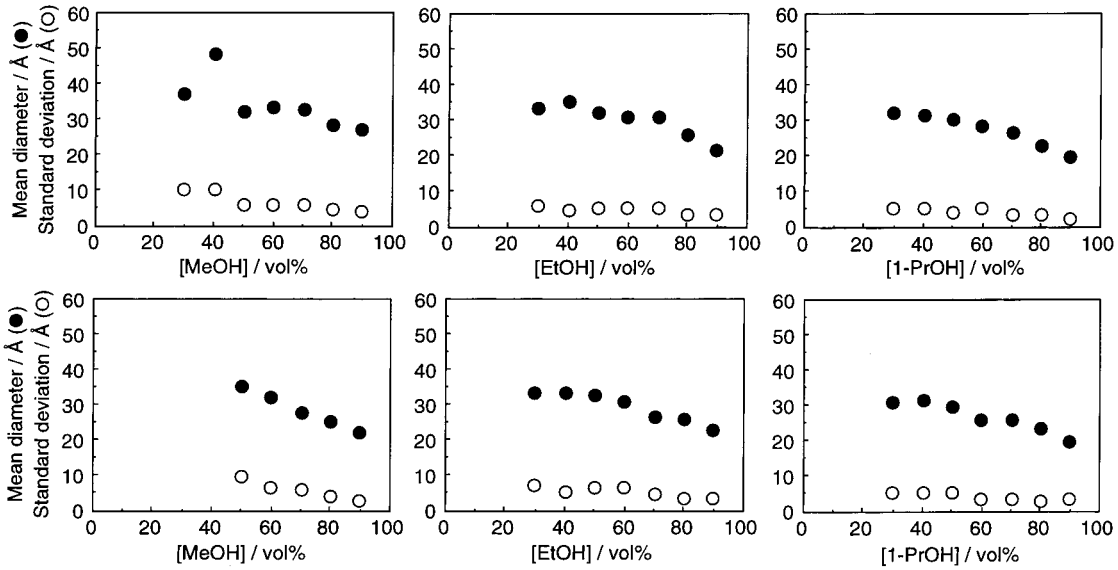

Figure 4. Mean diameters (●) and standard deviations (○) of PVP-Pt nanoparticles synthesized in alcohol/water mixed solvent under reflux for 3 h. PVP/Pt = 10 (upper) and 40 (lower).

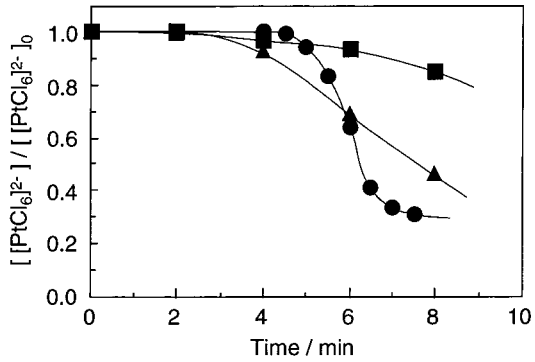

Figure 5. Influence of kind of alcohol on the reduction rate of $[PtCl_6]^{2-}$. (PVP/Pt = 10, [alcohol] = 90 vol %.) $[[PtCl_6]^{2-}]_0$ stands for an initial concentration of $[PtCl_6]^{2-}$ ions. (■) methanol; (▲) ethanol; (●) 1-propanol.

that the reduction of $[PtCl_6]^{2-}$ by the alcohol with higher boiling point produces more Pt nuclei in a shorter period and suppresses the growth of Pt nanoparticles, that is, a faster reduction rate of $[PtCl_6]^{2-}$ is needed to generate the smaller Pt nanoparticles with a narrower distribution.

In general, an increase in the concentration of the reducing agent increases the reduction rate of metal ions, leading to the formation of smaller metal nanoparticles. In fact, the smaller particles with a narrower size distribution were produced at the higher concentrations of alcohol, as shown in Figure 4, because both the PVP and H_2PtCl_6 completely disperse in an alcohol/water mixed solution. At lower concentrations of alcohol, both the PVP and H_2PtCl_6 homogeneously disperse in solution, but the reduction rate of $[PtCl_6]^{2-}$ decreases, especially in the case of methanol, resulting in the formation of larger particles. Consequently, the particle size gradually decreased with an increase in the concentration of alcohol. On the contrary, in the case of the PVP-protected Pd nanoparticles, a minimum in sizes of the Pd nanoparticles appeared at 20−40 vol % of alcohol by using H_2PdCl_4 as an alcohol-insoluble precursor.[45]

Duff et al.[44] previously mentioned that it was insufficient to refer only to the standard deviation in a particle size determination on a one-step reaction if one is trying to establish a correlation between particle size and preparative conditions. In fact, the samples with the standard deviation >5.0 Å (low alcohol concentrations) appear not to have the true global mean. However, the samples prepared at high alcohol concentrations such as 90 vol % are highly reproducible. For example, when the micrographs of Pt nanoparticles prepared in methanol/water (9/1, v/v) at PVP/Pt = 10 were recorded from three different areas of the same grid, the calculated mean diameters were within 27.4 ± 0.5 Å, with a similar Gaussian curve. Moreover, the diameters of three different samples were within 27.4 ± 1.0 Å, with a similar Gaussian curve. Taking the confidence limits into consideration, it was concluded that the Pt nanoparticles prepared at high alcohol concentration had the true global mean diameters, and we could establish a correlation between particle size and preparative conditions at high alcohol concentration such as 90 vol %.

Size Control of Pt Nanoparticles by Variation of the Amount of PVP. As shown in Figure 4, the size of the PVP-Pt nanoparticles is influenced by the amount of PVP. The protective polymer, PVP, apparently stabilizes the Pt nanoparticles by preventing them from aggregating. The coordination of N and O atoms of PVP to the surface Pt atoms of the Pt nanoparticles was confirmed by FT-IR and XPS measurements. Accordingly, the amount of PVP added to the solution is expected to affect the growth process for the Pt nanoparticles. Therefore, the change in size of the Pt nanoparticles was investigated by varying the amount of PVP at the high concentration of methanol. Figure 6 presents the TEM images of the PVP-Pt nanoparticles synthesized at various molar ratios of PVP/Pt in methanol/water (9/1, v/v) under reflux for 3 h. Decreasing the PVP/Pt ratio gives the larger Pt nanoparticles with a narrow size distribution, although the PVP/Pt ratio of 0.1 gave the Pt precipitates. The similar results were obtained in the case of ethanol and 1-propanol. With decreasing the PVP/Pt ratio, the growth of the particles is thought to proceed by the lack of the number of protecting groups of PVP. Therefore, the particle size can be significantly controlled by the kind of alcohol and the amount of PVP (PVP/Pt > 0.1) at the high concentration of alcohol, the size distribution remaining quite narrow.

In addition, the PVP-Pt nanoparticles synthesized at PVP/Pt = 1.0 tend to assemble themselves on carbon-coated Cu grid, as observed in Figure 6c. The detail is discussed later.

Influence of Molecular Weight of PVP on Size of Pt Nanoparticles. It is well known that the flexible polymers with a low degree of polymerization have extended polymer chains,

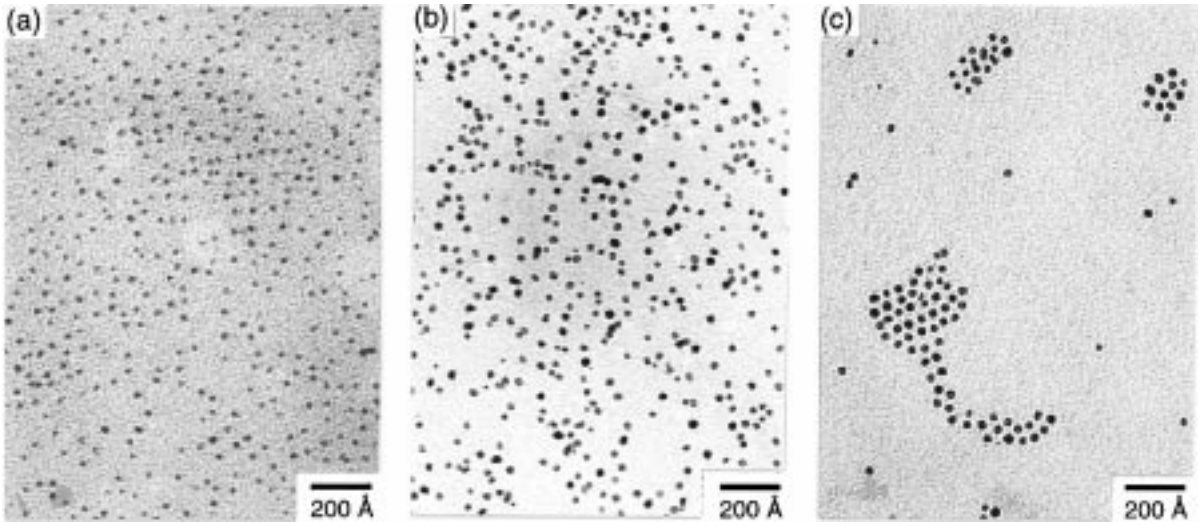

Figure 6. TEM images of the PVP-Pt nanoparticles synthesized in 90 vol % methanol solution at various PVP/Pt ratios. (a) PVP/Pt = 40 (d = 24.7 Å, σ = 3.07 Å), (b) 10 (d = 27.4 Å, σ = 4.11 Å), (c) 1.0 (d = 33.1 Å, σ = 3.28 Å).

TABLE 2: Mean Diameters and Standard Deviations of PVP-Pt Nanoparticles[a] Synthesized by Using Various M_w of PVP

M_w of PVP	mean diameter, Å	standard deviation, Å
10 000	30.0	2.36
29 000	31.1	2.28
40 000	33.1	3.28
55 000	33.3	1.62
1 300 000	32.5	1.87

[a] Synthesized in methanol/water (9/1, v/v) at molar ratio of PVP/Pt = 1.0.

whereas those with a high degree of polymerization adopt random-coil conformations in solution. To examine the influence of the chain conformation of PVP on the size of the Pt nanoparticles, they were synthesized in methanol/water (9/1, v/v) by using PVP of various M_w, 10 000, 29 000, 40 000, 55 000, and 1 300 000. The molar ratio of PVP/Pt was fixed to be 1.0. The mean diameters and standard deviations of the Pt nanoparticles protected by PVP of various M_w are summarized in Table 2. No remarkable influence of the chain conformation of PVP on the size of the Pt nanoparticles was observed, that is, the spherical Pt nanoparticles were distributed in the range from 22.5 to 40 Å with similar mean diameters. Therefore, it is concluded that the molar ratio of PVP to Pt is intrinsically important to control the size of the Pt nanoparticles, when using PVP of M_w over 10 000 as a protective agent.

Stepwise Growth and Growth Mechanism of Pt Nanoparticles. By using a one-step synthesis, one can obtain the Pt nanoparticles in the range 19−33 Å in mean diameter, whereas it is quite difficult to synthesize the Pt nanoparticles larger than 33 Å. Thus, the monodispersed PVP-Pt nanoparticles synthesized in a one-step reaction were used for stepwise growth to obtain nanoparticles larger than 33 Å without changing the size distribution. The PVP-Pt nanoparticles synthesized in methanol/water (9/1, v/v) at PVP/Pt = 1.0 have a mean diameter of 33.1 Å with a narrow size distribution (σ = 3.28 Å), and thus they were employed as the starting particles for stepwise growth. A second growth of PVP-Pt nanoparticles was carried out by mixing 25 mL of 0.6 mM PVP-Pt dispersion with 25 mL of 0.6 mM H_2PtCl_6 in methanol/water (9/1, v/v) solution, followed by refluxing the mixture for 3 h. A third growth was conducted in a similar manner. The TEM photographs and size distributions of PVP-Pt obtained at each growth step are shown in Figure 7. The nanoparticles are clearly growing with increasing growth steps, indicating that the nanoparticles in the solution serve as nuclei for larger ones. The diameter of nanoparticles to be obtained, d, can be calculated by eq 2[49]

$$d = d_0 \sqrt[3]{\frac{n_i + n_m}{n_m}} \tag{2}$$

where d_0 = particle diameter in the starting solution and n_i, n_m = quantity of the ionic and metallic Pt, respectively. In our case, $n_i = n_m$, so that the formula 2 leads to eq 3

$$d = \sqrt[3]{2}\, d_0 \tag{3}$$

The mean diameters of PVP-Pt estimated by the TEM photographs are 33.1, 41.2, and 50.1 Å, whereas those calculated from eq 3 are 33.1, 41.7, and 52.5 Å. The experimental results show a slightly smaller diameter than the calculated ones. The first particles are distributed from 22.5 to 40.0 Å. Assuming that each particle grows according to eq 3, the second and third particles are predicted to have size distributions from 28.3 to 50.4 Å and 35.7 to 63.5 Å, respectively. Those results are in good agreement with the experimental ones, indicating that the size distribution of the starting particles greatly influences that of the stepwise-synthesized particles. Therefore, the application of separation procedures, such as HPLC[50] or fractional precipitation,[10] to Pt nanoparticles obtained by a one-step reaction may be effective to synthesize larger particles with a narrow size distribution. Combination of the PVP-Pt nanoparticles synthesized in a one-step reaction as nuclei with arbitrary amounts of n_i enables us to obtain the monodispersed Pt nanoparticles of arbitrary diameter in the range 19−50 Å.

The shape distributions of these Pt nanoparticles obtained here were measured from enlarged TEM photographs (insets in size distribution diagrams in Figure 7). The truncated octahedral shapes are dominant with some percentages of irregular prismatic and cubic shapes in the first and second Pt nanoparticles, while the relative percentages of irregular prismatic and cubic particles, especially the former, increase in the third particles. Each sample contained few tetrahedral particles. Furlong et al.[51] proposed the use of a factor S calculated from the UV−vis spectrum, defined by eq 4, to characterize dispersions of Pt.

$$S = \frac{d(\log \text{extinction})}{d(\log \text{wavelength})} \tag{4}$$

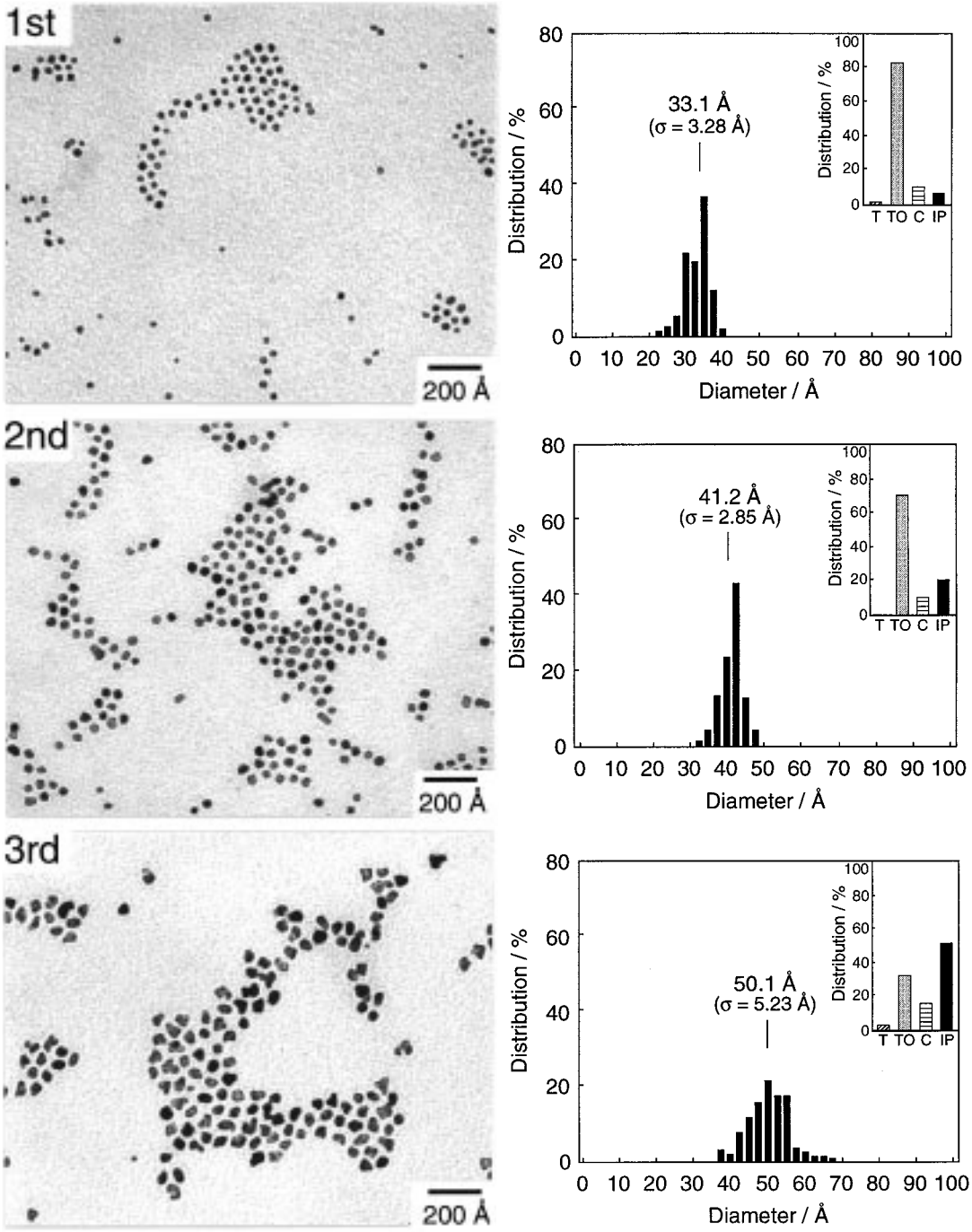

Figure 7. TEM images of PVP-Pt nanoparticles synthesized by the stepwise growth and size distributions estimated from the images (PVP/Pt = 1.0, [methanol] = 90 vol %). The insets in size distribution diagrams show the shape distributions of these particles, where T, TO, C, and IP on the horizontal axes stand for tetrahedral, truncated octahedral, cubic, and irregular prismatic particles, respectively.

They suggested that *S* decreased with increasing particle size. Duff et al.[44] reconsidered and concluded that *S* is a parameter of particulate shape, i.e., deviations from sphericity, as found in the morphology of partly coalesced coagulates, cause decrease in *S*. In our well-separated three samples prepared by the stepwise growth process, *S* values were calculated according to eq 4 with the gradient of the straight line fit over the wavelength region 400−600 nm. The double-log plots of the optical spectrum fitted well to straight lines with correlation coefficient $R^2 = 1.000$, and *S* values obtained were 2.94, 2.87, and 2.67 for first, second, and third particles, respectively. This decrease in *S* values indicates that the shape of the Pt nanoparticles deviated from the sphericity with the proceeding of the stepwise growth.

As Petroski and co-workers have recently revealed,[48] the shapes of the Pt nanoparticles are thought to be changed from truncated octahedra to irregular prisms and cubes during the growth process. The first Pt particles are dominant with the truncated octahedral shapes. The coordination of Pt^{4+} ions to PVP, which is protecting the Pt nanoparticles, may occur by the addition of Pt^{4+} to Pt nanoparticle suspension. Then, the Pt atoms produced by the reduction of Pt^{4+} aggregate on the surface of the Pt nanoparticles due to the formation of strong metallic bond. The {111} face grows faster than the other faces,[48] resulting in an increase in the percentages of irregular prismatic and cubic shapes for the second and third Pt particles. The third particles are especially dominant with these shapes. The fourth growth of PVP-Pt nanoparticles gave the Pt precipitate, since

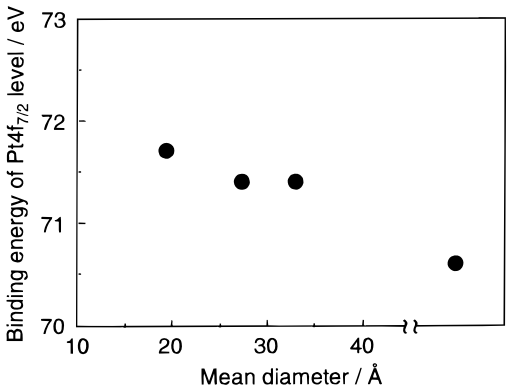

Figure 8. Binding energies of $Pt4f_{7/2}$ level of Pt black and PVP-Pt nanoparticles of different sizes.

the amount of PVP is not sufficient to protect the fourth growth Pt nanoparticle.

XPS Study on Pt Nanoparticles. Miniaturization of the particles affects not only the band structure formed by overlapping the valence electronic levels, but also the electronic state of the inner-shell electrons. The XPS measurements were conducted with four samples of different sizes to investigate an effect of the miniaturization of the particles on an electronic state of the inner-shell electrons. The samples employed here are Pt black and PVP-Pt nanoparticles of 19.4, 27.4, 33.1 Å in mean diameters synthesized in 1-propanol/water (9/1, v/v) at PVP/Pt = 10 (mol/mol), methanol/water (9/1) at PVP/Pt = 10, and methanol/water (9/1) at PVP/Pt = 1.0, respectively. Figure 8 shows the change in $Pt4f_{7/2}$ binding energies with increasing the particle size. As presented in Table 1, the N and O atoms of PVP slightly shifted toward higher binding energy, so that the surface Pt atoms coordinating to these atoms should be in an electron-rich state. Nevertheless, the $Pt4f_{7/2}$ binding energies of Pt nanoparticles are shifted toward higher binding energy than that of Pt black (+1.1, +0.8, +0.8 eV for 19.4, 27.4, and 33.1 Å Pt nanoparticles, respectively). These shift values have a tendency to become larger for the smaller nanoparticles, a tendency which was observed at the Au nanoparticles.[52] The holes formed by releasing the photoelectrons behave as the positive charges and are not effectively shielded by the electrons due to the discrete energy levels in the nanoparticles, resulting in increasing the binding energies.[53] The detail for quantitative discussion is under investigation.

Crystal Structure of Pt Nanoparticles. The crystal structures of Pt nanoparticles were examined by XRD, ED, and 300 kV HRTEM. The XRD patterns of Pt black and PVP-Pt nanoparticles with mean diameters of 33.1, 27.4, 22.3, and 21.6 Å are shown in Figure 9. Table 3 summarizes the diffraction angle, the half-width, and the interplanar spacing of {111} plane and the lattice constant. Several peaks were observed in each XRD pattern at 39.7, 46.2, 67.4, 81.2, and 85.7°, which correspond to {111}, {200}, {220}, {311}, and {222} of the fcc lattice, respectively.[49] Their bandwidth became broader with smaller particle size, whereas the lattice constant remained unchanged. Figure 10 presents the HRTEM images of first, second, and third growth particles synthesized by the stepwise growth reaction, together with the ED pattern of first particles. Each particle shows a lattice image, and the first and second particles are concluded to be single crystallites. It is interesting to note that the third particles contain a small amount of the twin particles having two crystallographic axes. Since 15 {111} layers are mainly observed in the first particles, they are concluded to have a 7-shell structure. In the second and third particles, 19 and 23 {111} layers corresponding to 9- and 11-shell structures

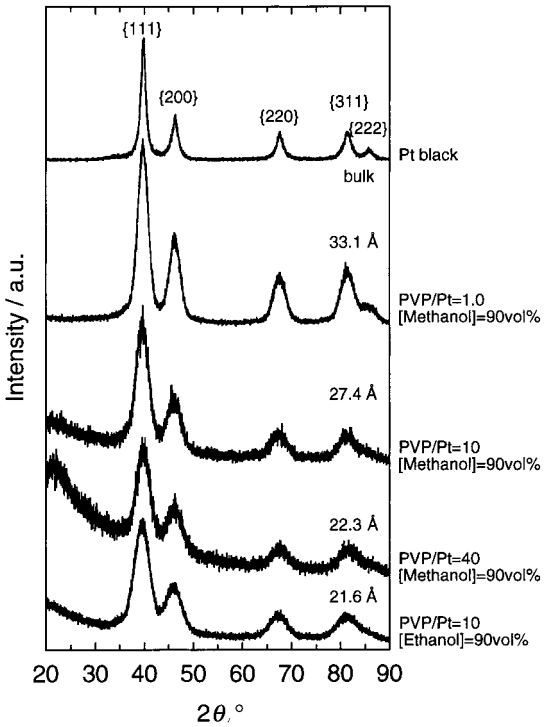

Figure 9. X-ray diffraction patterns of Pt black and PVP-Pt nanoparticles of various sizes.

TABLE 3: Diffraction Angle, Half-Width, Interplanar Spacing of {111} Plane, and Lattice Constant of PVP-Pt Nanoparticles of Various Diameters

synthetic condition	mean diameter	2θ of {111}, deg	Δ2θ of {111}[a], deg	d^b, Å	a^c, Å
Pt black		39.78	0.92	2.2640	3.9214
PVP/Pt = 1.0 [methanol] = 90 vol %	33.1	39.68	2.63	2.2695	3.9309
PVP/Pt = 10 [methanol] = 90 vol %	27.4	39.62	3.13	2.2728	3.9366
PVP/Pt = 40 [methanol] = 90 vol %	22.3	39.84	3.33	2.2607	3.9157
PVP/Pt = 10 [ethanol] = 90 vol %	21.6	39.76	3.51	2.2651	3.9233

[a] Half-width of {111} peak. [b] {111} interplanar spacing. [c] Lattice constant.

are often observed, respectively, which is reasonable, taking the amount of $H_2[PtCl_6]$ added in stepwise growth step into consideration. The lattice spacing, 2.3 Å, is in good agreement with that of bulk Pt.[54] Selected area ED showed four Debye−Scherrer rings assigned to {111}, {200}, {220}, and {311} planes, which supported the XRD results. Therefore, PVP-Pt nanoparticles synthesized in the present study have such face-centered cubic (fcc) structures as bulk Pt.

Electrophoretic Deposition of Pt Nanoparticles on Electrode. In Figure 7, the Pt nanoparticles (PVP/Pt below 1.0) tend to assemble themselves, although the self-assembly is not observed in those synthesized at PVP/Pt ratios over 10. Thickness of PVP layer protecting the Pt nanoparticles is thought to affect their organization, that is, the flexibility of PVP around the particles would be suppressed in the case of PVP/Pt below 1.0. However, expanding the area of Pt nanoparticle monolayer by self-assembly technique is too difficult, and thus we used an electric field as an external force to obtain Pt nanoparticle monolayer with wide region, making use of negatively charged Pt nanoparticles.

At first, an electrophoretic deposition (EPD) of 33.1 Å PVP-Pt nanoparticles was carried out in different compositions of

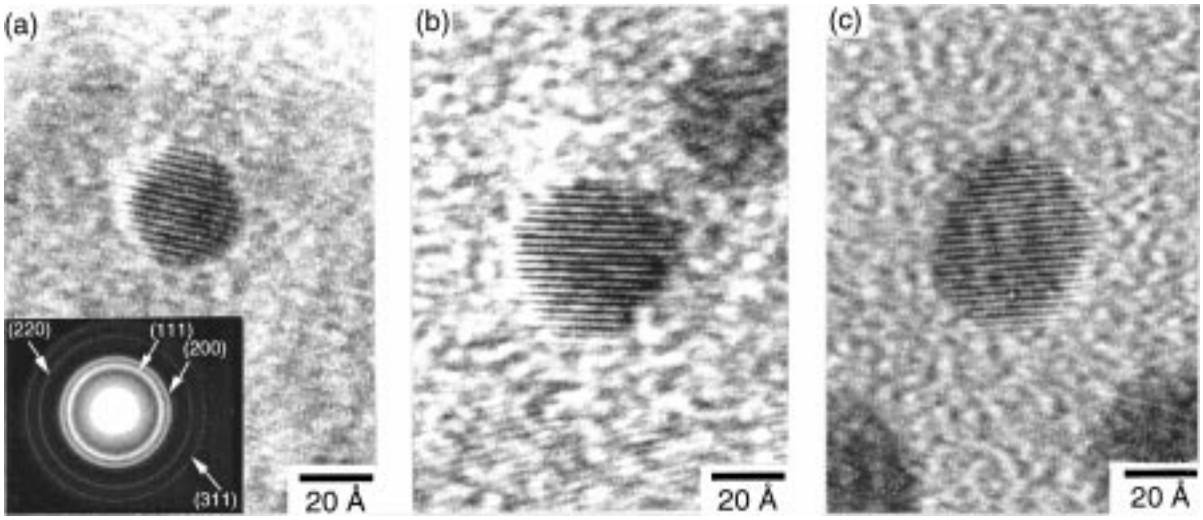

Figure 10. HRTEM images and ED pattern of PVP-Pt nanoparticles synthesized by the stepwise growth reaction shown in Figure 9.

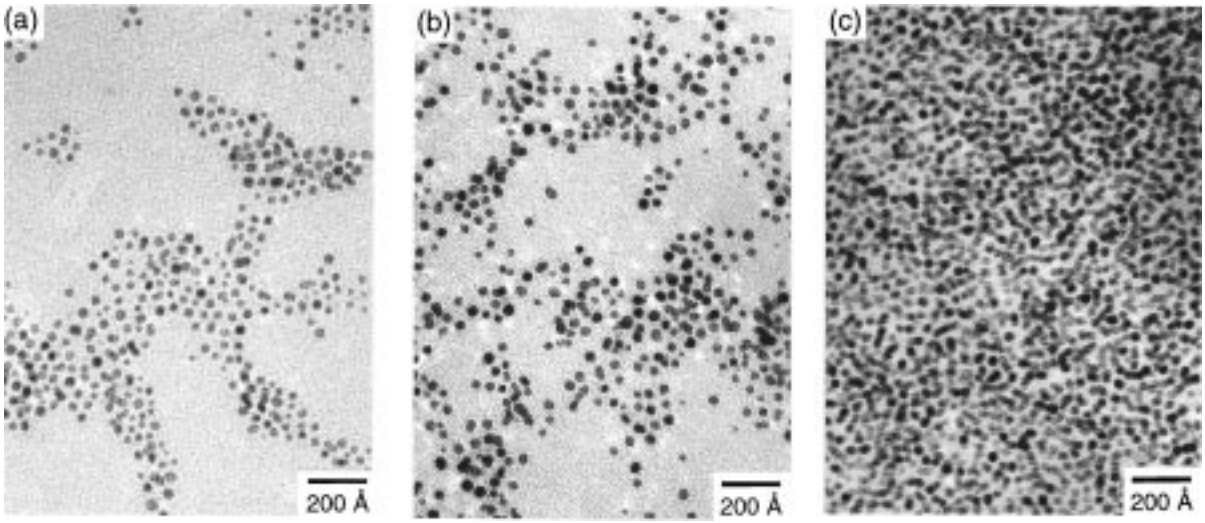

Figure 11. Electrophoretic deposition of 33.1 Å PVP-Pt nanoparticles in methanol/water mixed solvent at 10 Vcm^{-1} for 20 min. The weight ratios of methanol/water are (a) 5/5, (b) 7/3, and (c) 10/0.

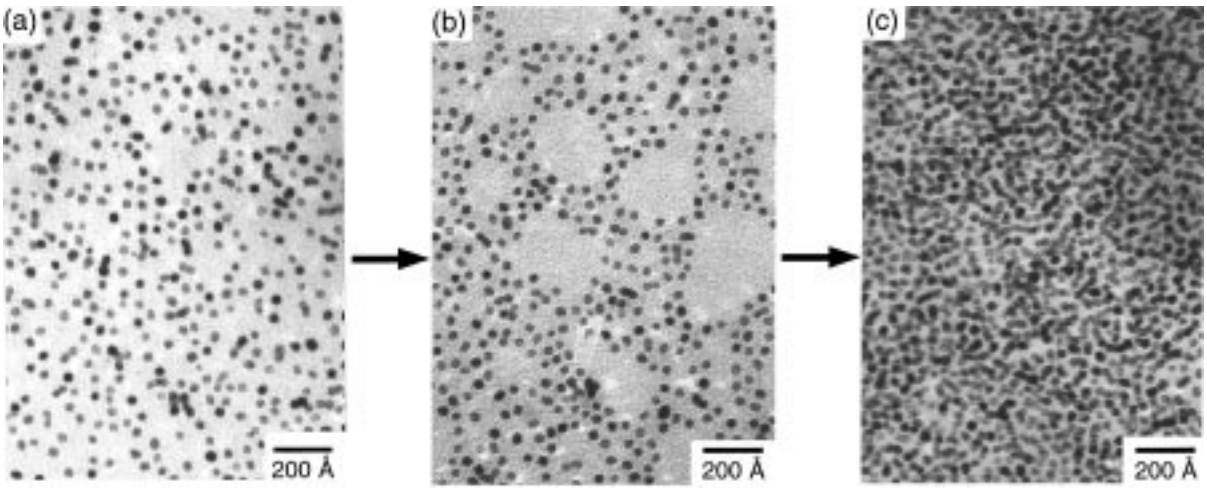

Figure 12. TEM images of 33.1 Å Pt nanoparticle monolayers prepared on carbon-coated copper grid after different electrophoretic time at 10 V cm^{-1}. The electrophoretic times are (a) 1 min, (b) 5 min, and (c) 20 min.

methanol/water mixed solvent (5/5, 7/3, and 10/1 (w/w), their viscosities being 1.534, 1.218, and 0.541 mPa s at 25 °C) to examine an influence of the viscosity of the solvent on the deposition rate of the particles. In general, when an electric field was applied to the particles with surface charges, they move against the Stokes resistance. The particles start a uniform motion in a liquid when these two forces are balanced according to the following eq 5[55]

$$QE = 6\pi\eta a v \tag{5}$$

where Q is the surface charge of the particle, E is the strength

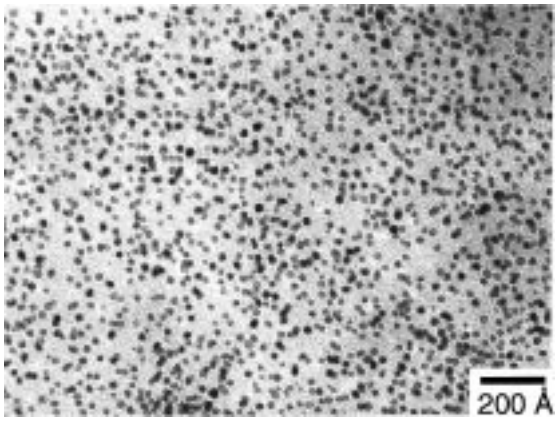

Figure 13. TEM images of 27.4 Å Pt nanoparticle monolayers prepared on carbon-coated copper grid at 10 V cm^{-1} for 60 min.

of the electric field, η is the viscosity of the liquid, a is the diameter of the particle, and v is the velocity of the particle. The influence of diffusion electric double layer is disregarded to simplify the system. v should be in inverse proportional to η. As presented in Figure 11, more Pt nanoparticles are deposited on the grid at higher concentration of methanol, indicating that the Pt nanoparticles can be deposited effectively in the solvent of lower viscosity. The number of Pt nanoparticles in unit area deposited in methanol is roughly 3 times as many as that in other two mixed solvents with comparable viscosities. Using ethanol instead of methanol gave a similar result. Therefore, EPD experiment was conducted in methanol afterward.

Figure 12 shows the growth of 33.1 Å Pt monolayer by varying the electrophoretic time at 10 V cm^{-1} in methanol. A completely new grid was used for each experiment. After 1 min, Pt nanoparticles randomly distributed on the grid as the isolated particles. After 5 min, Pt nanoparticles clearly began to assemble in two-dimensional network around the carbon-coated copper grid. After 20 min, the grid was largely covered with the Pt nanoparticles, and the Pt nanoparticle monolayer was formed, although the multilayer was partly observed. Pt particles (33.1 Å) showed similar behavior at 5−25 V cm^{-1}, and the higher the applied voltage was, the faster the Pt nanoparticles moved according to eq 5. However, the electrophoretic time over 20 min gives the multilayer of Pt nanoparticles around the grid at the electric field over 10 V cm^{-1}. As Giersig et al.[29] pointed out, attractive surface forces may exist between the deposited Pt nanoparticles. Although the presence of the network structure at 5 min of electrophoretic time implies that the nanoparticles are mobile on the surface of the grid and tend to aggregate in two-dimensions, the attractive surface forces between the PVP-Pt nanoparticles are not so strong as those between the ligand-stabilized Au nanoparticles.[29]

When 27.4 Å PVP-Pt nanoparticles were used for an EPD, they also assembled densely with increasing the applied voltage and the electrophoretic time as well as 33.1 Å PVP-Pt. At 10 V cm^{-1}, however, they were not densely deposited on the grid even after 60 min of an electrophoretic time (Figure 13). If the particles behave according to eq 5, they ought to move toward the anode faster than 33.1 Å ones, probably because the nanoparticles of smaller size tend to have less negative charge, resulting in decreasing the deposition rate of 27.4 Å Pt nanoparticles on the grid compared with 33.1 Å ones.

Then, the influence of the concentration of Pt nanoparticles on the arrangement was examined. As shown in Figure 14a, an EPD of 0.6 mM dispersion of 33.1 Å Pt nanoparticles at 5 V cm^{-1} for 20 min left many vacancies on a grid and did not form the Pt nanoparticle monolayer. As might be anticipated, with 6.0 mM dispersion of Pt nanoparticles in place of 0.6 mM dispersion, a dense Pt nanoparticle monolayer was formed even at 5 V cm^{-1} for 5 min due to an increase in the number of the Pt nanoparticles in unit volume, as shown in Figure 14b. The ratio of the number of Pt nanoparticles deposited in unit area under EPD conditions adopted in Figure 14a different from those in Figure 14b is roughly 4/10, which value is compatible with the ratio estimated by eq 5. Therefore, the high concentration of Pt dispersions was preferable for ordering monodispersed Pt nanoparticles effectively. However, the formation of the Pt nanoparticle monolayer in a completely hexagonal network has not yet been achieved. Moreover, the coalescence of the

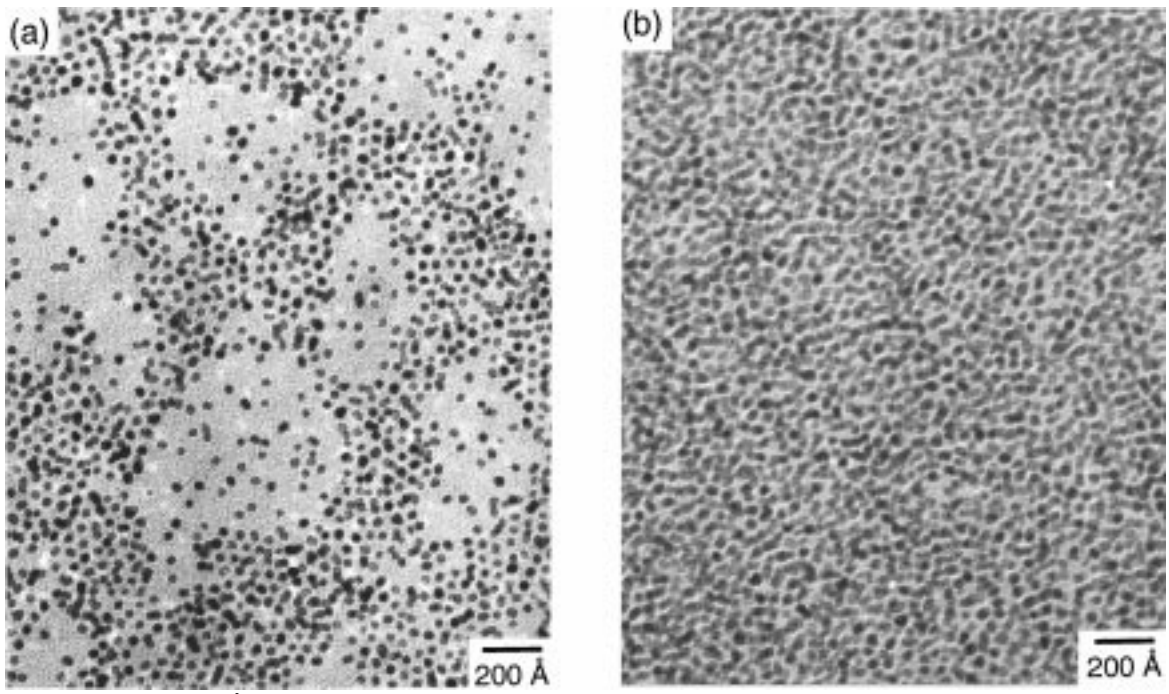

Figure 14. TEM images of 33.1 Å Pt nanoparticle monolayers prepared on carbon-coated copper grid by electrophoretic deposition of (a) a 0.6 mM Pt particle dispersion at 5 V cm^{-1} for 20 min and (b) a 6.0 mM Pt particle dispersion at 5 V cm^{-1} for 5 min.

particles, which may result from intertwining of the swelling polymer in methanol at high Pt concentration, was observed. The careful adjustment of both the concentration of Pt nanoparticles and the composition of solvent should be taken into consideration to form the closest packed Pt monolayer in a hexagonal network.

Conclusions

In this research, we established the method to control the size of Pt nanoparticles in the range 19−50 Å by combining a one-step reaction with a stepwise growth reaction. In one-step reaction, the nucleation rate was the principal factor in determining the particle size and distribution, i.e., using alcohol with higher boiling point at higher alcohol concentration gives smaller and narrower distributed Pt nanoparticles. In the viewpoint of PVP, what influenced the size of Pt nanoparticles was not the molecular weight but the molar ratio of PVP to Pt. Larger particles with a narrow size distribution were easily available by growing the monodispersed particles obtained with a one-step reaction, where the growth rate on {111} faces may be faster than that on {100} faces, resulting in a distribution dominated with the irregular prismatic and cubic shapes. The quantum size effect was revealed by XPS measurement as the shift of $Pt4f_{7/2}$ level resulting from the discrete valence electronic levels of the nanoparticles. The Pt nanoparticles synthesized in the present study had such fcc structures as bulk Pt, the lattice constant being unchanged with a decrease in the particle size. With an electrophoretic deposition, 33.1 Å Pt nanoparticles moved faster toward the anode in solvent of lower viscosity, and more particles assembled on an anode with increasing both the applied voltage and the electrophoretic time to form the Pt nanoparticle monolayer Pt nanoparticles (27.4 Å) showed a similar behavior, although they gradually assembled on the anode presumably due to less negative charge. Using the solution with a higher concentration of Pt nanoparticles effectively provided the close Pt nanoparticle monolayer in the wide region. Our next aims are to control the shape of the nanoparticles and to assemble them in a hexagonal network.

Acknowledgment. The present work was partially supported by a Grant-in-Aid for Scientific Research in Priority Areas of "New Polymers and Their Nano-organized Systems" (No. 277/10126224) and for Encouragement of Young Scientists (No. 09740519) from the Ministry of Education, Science, Sports and Culture, Japan.

References and Notes

(1) *Clusters and Colloids*; Schmid, G., Ed.; VCH: Weinheim, 1994.

(2) Volokitin, Y.; Sinzig, J.; de Jong, L. J.; Schmid, G.; Vargaftik, M. N.; Moiseev, I. I. *Nature* **1996**, *384*, 621.

(3) Colvin, V. L.; Schlamp, M. C.; Alivisatos, A. P. *Nature* **1994**, *370*, 354.

(4) Pileni, M. P. *J. Phys. Chem.* **1993**, *97*, 6961.

(5) (a) Bradley, J. S. *Clusters and Colloids*, Schmid, G., Ed.; VCH: Weinheim, 1994; Chapter 6. (b) Köhler, J. U.; Bradley, J. S. *Catal. Lett.* **1997**, *45*, 203.

(6) Lewis, L. N. *Chem. Rev.* **1993**, *93*, 2693.

(7) Bönnemann, H.; Brijoux, W.; Brinkmann, R.; Fretzen, R.; Joussen, T.; Köppler, R.; Korall, B.; Neiteler, P.; Richter, J. *J. Mol. Catal.* **1994**, *86*, 129.

(8) (a) Hirai, H.; Toshima, N. In *Tailored Metal Catalysts*; Iwasawa, Y., Ed.; D. Reidel: Dordrecht, The Netherlands, 1986; pp 87−140. (b) Toshima, N.; Shiraishi, Y.; Miyake, M.; Teranishi, T.; Tominaga, T.; Bönnemann, H.; Brijoux, W.; Schmid, G., manuscript in preparation.

(9) Halperin, W. P. *Rev. Mod. Phys.* **1986**, *58*, 533.

(10) Taleb, A.; Petit, C.; Pileni, M. P. *Chem. Mater.* **1997**, *9*, 950.

(11) Motte, L.; Billoudet, F.; Lacaze, E.; Douin, J.; Pileni, M. P. *J. Phys. Chem. B* **1997**, *101*, 138.

(12) Fendler, J. H.; Meldrum, F. C. *Adv. Mater.* **1995**, *7*, 607.

(13) Herron, N.; Wang, Y.; Eddy, M.; Stucky, G. D.; Cox, D. E.; Moller, K.; Bein, T. *J. Am. Chem. Soc.* **1989**, *111*, 530.

(14) Brust, M.; Walker, D.; Bethell, D.; Schiffrin, D. J.; Whyman, R. *J. Chem. Soc., Chem. Commun.* **1994**, 801.

(15) Murray, C. B.; Norris, D. J.; Bawendi, M. G. *J. Am. Chem. Soc.* **1993**, *115*, 8706.

(16) Freeman, R. G.; Grabar, K. C.; Allison, K. J.; Bright, R. M.; Davis, J. A.; Guthrie, A. P.; Hommer, M. B.; Jackson, M. A.; Smith, P. C.; Walter, D. G.; Natan, M. J. *Science* **1995**, *267*, 1629.

(17) Terrill, R. H.; Postlethwaite, T. A.; Chen, C.; Poon, C.-D.; Terzis, A.; Chen, A.; Huthison, J. E.; Clark, M. R.; Wignall, G.; Londono, J. D.; Superfine, R.; Falvo, M.; Johnson, C. S., Jr.; Samulski, E. T.; Murray, R. W. *J. Am. Chem. Soc.* **1995**, *117*, 12537.

(18) Alivasatos, A. P. *Science* **1996**, *271*, 933.

(19) Xia, Y.; Kim, E.; Mrksich, M.; Whitesides, G. M. *Chem. Mater.* **1996**, *8*, 601.

(20) Kumar, A.; Whitesides, G. M. *Science* **1994**, *263*, 60.

(21) Hinz, P.; Dislich, H. J. *Non-Cryst. Solids* **1986**, *82*, 411.

(22) Hahn, R. E.; Seraphin, B. O. In *Physics of Thin Film*; Academic Press: New York, 1978.

(23) Kastner, M. A. *Phys. Today* **1993**, 24.

(24) Harfenist, S. A.; Wang, Z. L.; Alvarez, M. M.; Vezmar, I.; Whetten, R. L. *J. Phys. Chem.* **1996**, *100*, 13904.

(25) Sarathy, K. V.; Kulkarni, G. U.; Rao, C. N. R. *Chem. Commun.* **1997**, 537.

(26) Reetz, M. T.; Winter, M.; Tesche, B. *Chem. Commun.* **1997**, 147.

(27) Fink, J.; Kiely, C. J.; Bethell, D.; Schiffrin, D. J. *Chem. Mater.* **1998**, *10*, 922.

(28) Taleb, A.; Petit, C.; Pileni, M. P. *J. Phys. Chem. B* **1998**, *102*, 2214.

(29) (a) Giersig, M.; Mulvaney, P. *J. Phys. Chem.* **1993**, *97*, 6334. (b) Giersig, M.; Mulvaney, P. *Langmuir* **1993**, *9*, 3408.

(30) Meldrum, F. C.; Kotov, N. A.; Fendler, J. H. *Langmuir* **1994**, *10*, 2035.

(31) Mirkin, C. A.; Letsinger, R. L.; Mucic, R. C.; Storhoff, J. J. *Nature* **1996**, *382*, 607.

(32) Dabbousi, B. O.; Murray, C. B.; Rubner, M. F.; Bawendi, M. G. *Chem. Mater.* **1994**, *6*, 216.

(33) Murray, C. B.; Kagan, C. R.; Bawendi, M. G. *Science* **1995**, *270*, 1335.

(34) Scoberg, D.; Grieser, F.; Furlong, D. N. *J. Chem. Soc., Chem. Commun.* **1991**, 515.

(35) Kotov, N. A.; Meldrum, F. C.; Wu, C.; Fendler, J. H. *J. Phys. Chem.* **1994**, *98*, 2735.

(36) Hu, K.; Brust, M.; Bard, A. J. *Chem. Mater.* **1998**, *10*, 1160.

(37) Kotov, N. A.; Meldrum, F. C.; Fendler, J. H. *J. Phys. Chem.* **1994**, *98*, 8827.

(38) Meldrum, F. C.; Kotov, N. A.; Fendler, J. H. *Chem. Mater.* **1995**, *7*, 1112.

(39) Teranishi, T.; Hosoe, M.; Miyake, M. *Adv. Mater.* **1997**, *9*, 65.

(40) Ahmadi, T. S.; Wang, Z. L.; Green, T. C.; Henglein, A.; El-Sayed, M. A. *Science* **1996**, *272*, 1924.

(41) Tanori, J.; Pileni, M. P. *Langmuir* **1997**, *13*, 639.

(42) (a) Hirai, H.; Nakao, Y.; Toshima, N. *J. Macromol. Sci., Chem.* **1978**, *A12*, 1117. (b) Hirai, H. *J. Macromol. Sci., Chem.* **1979**, *A13*, 633. (c) Hirai, H.; Chawanya, H.; Toshima, N. *React. Polym.* 1**985**, *3*, 127.

(43) (a) Bradley, J. S.; Millar, J. M.; Hill, E. W. *J. Am. Chem. Soc.* **1991**, *113*, 4016. (b) Bradley, J. S.; Hill, E. W.; Behal, S.; Klein, C.; Chaudret, B.; Duteil, A. *Chem. Mater.* **1992**, *4*, 1234.

(44) Duff, D. G.; Edwards, P. P.; Johnson, B. F. G. *J. Phys. Chem.* **1995**, *99*, 15934.

(45) Teranishi, T.; Miyake, M. *Chem. Mater.* **1998**, *10*, 594.

(46) Teranishi, T.; Hori, H.; Miyake, M. *J. Phys. Chem. B* **1997**, *101*, 5774.

(47) Teranishi, T.; Kiyokawa, I.; Miyake, M. *Adv. Mater.* **1998**, *10*, 596.

(48) Petroski, J. M.; Wang, Z. L.; Green, T. C.; El-Sayed, M. A. *J. Phys. Chem. B* **1998**, *102*, 3316.

(49) Schmid, G. *Chem. Rev.* **1992**, *92*, 1709.

(50) Henglein, A. *J. Phys. Chem.* **1993**, *97*, 5457.

(51) Furlong, D. N.; Launikonis, A.; Sasse, W. H. F.; Sanders, J. V. *J. Chem. Soc., Faraday Trans. 1* **1984**, *80*, 571.

(52) Oberli, L.; Monat, R.; Matieu, H. J.; Landolt, D.; Buttet, J. *Surf. Sci.* **1981**, *106*, 301.

(53) Kirschner, J. *Top. Curr. Phys.* **1977**, *4*, 59.

(54) JCPDS-ICDD, PDF-2 Data Base.

(55) *Zeta Potential*; Kitahara, F.; Furusawa, K.; Ozaki, M.; Ohshima, H.; Scientist: Tokyo, 1995; p.6.